Journal of Hydroscience and Hydraulic Engineering
Vol. 8, No. 1, October, 1990, 31-40

Numerical Simulation of Density Underflow by the $k - \varepsilon$ Turbulence Model

by
Yusuke Fukushima and Masami Watanabe
Nagaoka University of Technology
Nagaoka, Niigata, Japan

SYNOPSIS

The turbulent structure of density underflow is investigated theoretically. The standard $k - \varepsilon$ turbulence model is adopted in the numerical model. The partial differential equations are discretized by the SIMPLE method in order to carry out the numerical calculation. The turbulent properties such as the kinetic energy of turbulence, Reynolds stresses, viscous dissipation rate of turbulence and eddy viscosity are simulated by the numerical analysis and compared with the experimental data. The whole reservoir is considered to be the calculational domain. Thus the inverse flow resulting from the entrainment of the upper water is taken into account. It is shown that the numerical model explains well the mean flow properties such as the distributions of velocity and salinity concentration.

[Key words: density current/$k - \varepsilon$ turbulence model/numerical analysis]

Introduction

Inflow water whose density is heavier than that of the ambient water in a reservoir flows down along the inclined boundary and forms density underflow. This phenomenon is often observed in nature and is important from an engineering point of view. The density underflow consists of the head region and the steady flow region at the upstream of the head region. The steady flow region consists of the flow development region near the entrance of the reservoir and the flow establishment region where the flow is fully developed.

The turbulent inclined wall plume and related phenomena were investigated by many researchers. The classical approach to these problem are made by Ellison and Turner [1]. They have measured distributions of velocity and concentration and indicated that the mechanism of entrainment of ambient fluid into plume is an important phenomenon. Tsubaki and Komatsu [2] have carried out the experiment similar to that of Ellison and Turner. They have described the mechanism of the entrainment of ambient water theoretically. Recently, various type of turbulence models, especially $k - \varepsilon$ turbulence model, are developed and widely used (Rodi [3]). Ljuboya and Rodi [4] have analysed the vertical wall plume by the algebraic Reynolds stress model and compared with Grella and Faeth's [5] experimental data. Sini and Dekeyser have analysed the plane jet and the axisymmetric jet by the $k - \varepsilon$ turbulence model. Murota et al. [7] have examined the applicability of turbulence models to a two-dimensional buoyant surface jet. They concluded that $k - \varepsilon$ turbulence model cannot explain the anisotropy of tuebulence and the algebraic Reynolds stress model can agree well with experimental data. The $k - \varepsilon$ turbulence model is the simplest two-equation turbulence model and it has only several adjusment parameters. The other turbulence model is more complicated and has many parameters to be determined.

Fukushima [8] showed that the flow establishment region has the similarity solutions using the $k - \varepsilon$ turbulence model and this similarity solution explains well distributions of velocity and density on the wide range of the hydraulic conditions and the channel slope. Fukushima

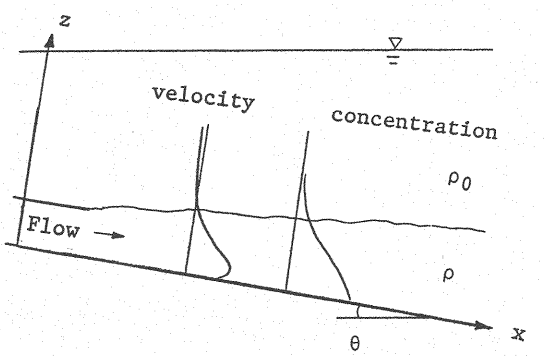

Fig. 1 Density underflow along the inclined wall.

and Takashima [9],[10] have carried out the numerical analysis using $k-\varepsilon$ turbulence model to investigate flow properties of the flow development region. We also have measured the turbulence quantities by the two-velocity component laser doppeler anemometer. Fukushima and Takashima [11] have compared the measured values with the similarity solutions for the flow establishment region and shown that the agreement of the similarity solutions with observed velocity, relative density difference, kinetic energy of turbulence, Reynolds stresses and eddy viscosity is fairly well. However, the analyses of Fukushima [8] and Fukushima and Takashima [9], [10] are restricted in the main body of jets, and the inverse flow resulting from the entrainment of ambient water is not taken into account.

In this paper, the numerical analysis is carried out for the whole domain of a reservoir in order to consider the inverse flow resulting from the water entrainment. The standard type of the $k-\varepsilon$ turbulence model connected with the diffusion equation of concentration of saline water is adopted in the numerical analysis [3]. The set of equations is discretized by the SIMPLE method developed by Patankar [12].

Fundamental equations of density underflow

Consider that the heavy water whose density is larger than that of ambient water in a reservoir flows down along the inclined solid boundary as shown in Fig. 1. The flow is two-dimensional, well developed turbulent flow. The density is considered to be the only function of concentration of salinity. The x coordinate is taken to the direction along the inclined bed and the z coordinate is taken to the direction normal to the x coordinate. u and w are the velocity components corresponding to the x and z coordinates, respectively. θ is the slope angle of the inclined boundary to the horizontal plane. The continuity equation of water, the momentum equations in the x and z directions, the diffusion equation of salinity c, the equation of kinetic energy of turbulence, k, and the equation of the viscous dissipation rate of turbulence, ε, are expressed as follows:
Continuity equation:

$$\frac{\partial u}{\partial x}+\frac{\partial w}{\partial z}=0 \tag{1}$$

Momentum equation in the x direction:

$$\frac{\partial u}{\partial t}+\frac{\partial}{\partial x}\left\{u^2-(\nu+\nu_t)\frac{\partial u}{\partial x}\right\}+\frac{\partial}{\partial z}\left\{uw-(\nu+\nu_t)\frac{\partial u}{\partial z}\right\}$$

$$=Rcg\sin\theta-\frac{\partial}{\partial x}\int_z^h Rcdzg\cos\theta-\frac{1}{\rho_o}\frac{\partial p'}{\partial x}+\frac{\partial}{\partial x}\left(\nu_t\frac{\partial u}{\partial x}\right)+\frac{\partial}{\partial z}\left(\nu_t\frac{\partial w}{\partial x}\right) \tag{2}$$

Momentum equation in the z direction:

Table 1: Numerical constants in the $k-\varepsilon$ turbulence model.

c_μ	σ_k	σ_ε	σ_t	$c_{1\varepsilon}$	$c_{2\varepsilon}$	$c_{3\varepsilon}$
0.09	1.0	1.3	0.8	1.44	1.92	1.0

$$\frac{\partial w}{\partial t}+\frac{\partial}{\partial x}\left\{uw-(\nu+\nu_t)\frac{\partial w}{\partial x}\right\}+\frac{\partial}{\partial z}\left\{w^2-(\nu+\nu_t)\frac{\partial w}{\partial z}\right\}$$

$$=-\frac{1}{\rho_o}\frac{\partial p'}{\partial z}+\frac{\partial}{\partial x}\left(\nu_t\frac{\partial u}{\partial z}\right)+\frac{\partial}{\partial z}\left(\nu_t\frac{\partial w}{\partial z}\right) \tag{3}$$

Diffusion equation of salinity:

$$\frac{\partial c}{\partial t}+\frac{\partial}{\partial x}\left\{uc-\left(D+\frac{\nu_t}{\sigma_t}\right)\frac{\partial c}{\partial x}\right\}+\frac{\partial}{\partial z}\left\{wc-\left(D+\frac{\nu_t}{\sigma_t}\right)\frac{\partial c}{\partial z}\right\}=0 \tag{4}$$

$k-$equation:

$$\frac{\partial k}{\partial t}+\frac{\partial}{\partial x}\left\{uk-\frac{\nu_t}{\sigma_k}\frac{\partial k}{\partial x}\right\}+\frac{\partial}{\partial z}\left\{wk-\frac{\nu_t}{\sigma_k}\frac{\partial k}{\partial z}\right\}$$

$$=\nu_t\left(\frac{\partial u}{\partial z}\right)^2+Rg\cos\theta\frac{\nu_t}{\sigma_t}\frac{\partial c}{\partial z}-\varepsilon \tag{5}$$

$\varepsilon-$equation:

$$\frac{\partial \varepsilon}{\partial t}+\frac{\partial}{\partial x}\left\{u\varepsilon-\frac{\nu_t}{\sigma_\varepsilon}\frac{\partial \varepsilon}{\partial x}\right\}+\frac{\partial}{\partial z}\left\{w\varepsilon-\frac{\nu_t}{\sigma_\varepsilon}\frac{\partial \varepsilon}{\partial z}\right\}$$

$$=c_{1\varepsilon}\frac{\varepsilon}{k}\left\{\nu_t\left(\frac{\partial u}{\partial z}\right)^2+(1-c_{3\varepsilon})Rg\cos\theta\frac{\nu_t}{\sigma_t}\frac{\partial c}{\partial z}\right\}-c_{2\varepsilon}\frac{\varepsilon^2}{k} \tag{6}$$

where g is the gravity acceleration, R is the ratio of the relative density difference to the concentration of the salinity, p' is the pressure deviation from the hydrostatic pressure distribution, ν is the kinematic viscosity and D is the molecular diffusivity. The eddy viscosity ν_t is expressed by

$$\nu_t=c_\mu\frac{k^2}{\varepsilon} \tag{7}$$

In Eq.(3), the gravity term is ommited because of the assumption of the hydro-static pressure distribution in Eq.(2). If the eddy viscosity is a constant, the last two terms of both Eqs.(2) and (3) can be neglected. The coefficients included in Eqs. (4),(5),(6) and (7),c_μ , σ_k , σ_ε , σ_t , $c_{1\varepsilon}$, $c_{2\varepsilon}$ and $c_{3\varepsilon}$ are numerical constants as shown in Table 1. The values of coefficients except for σ_t and $c_{3\varepsilon}$ are determined using experimental data of various type of flow (e.g. Rodi[3]). Fukushima [8] has discussed the values of σ_t and $c_{3\varepsilon}$ for the inclined wall plume. The likely values of σ_t and $c_{3\varepsilon}$ are shown in Table 1. There are some arguments on the value of parameter c_μ, σ_t, $c_{3\varepsilon}$. For example, σ_t and $c_{3\varepsilon}$ may be dependent on the condition of stratification. In this calculation, c_μ, σ_t and $c_{3\varepsilon}$ are treated as constants. However, more detailed discussion on the values of coefficients will be necessary.

Next, the boundary conditions are considered.

(a) the boundary conditions at the entrance section: u, c and k are decided based on the experimental values at the entrance section. The distribution of ε is calculated by equation (7) using the experimental values of k and ν_t . The distributions of w and p' are given as

$$w=0 \tag{8}$$

$$p' = 0 \tag{9}$$

(b) the boundary conditions at the exit section: It is assumed that the flow is uni-directional so that u, c, k and ε is independent from the exit section. The distributions of w and p' are given as

$$w = 0 \tag{10}$$

$$p' = 0 \tag{11}$$

(c) the boundary conditions at the inclined wall: The log law of velocity distribution and the local equilibrium of turbulence are assumed in the wall boundary conditions. Thus the wall function method which is widely adopted in the turbulence model will be assumed as follows:

$$\frac{u_o}{u_*} = \frac{1}{\kappa} \ln \left(\frac{z_o u_*}{\nu} \right) + A_s \tag{12}$$

$$w = 0 \tag{13}$$

$$\frac{k}{u_*^2} = \frac{1}{\sqrt{c_\mu}} \tag{14}$$

$$\varepsilon = \frac{u_*^3}{\kappa z_o} \tag{15}$$

$$\frac{\partial c}{\partial z} = 0 \tag{16}$$

where z_o is the height from the wall, u_* is the friction velocity at the wall, κ is the Kármán constant and $A_s (= 5.5)$ is a numerical constant. We apply Eq.(12) to two points near the wall. Thus u_* and u_0, where u_0 is the velocity at $z = z_0$, will satisfy Eq.(12). The shear velocity u_* can be obtained in the process of the iteration of calculations.

(d) the boundary conditions at the water surface: The derivatives of u, c, k and ε with respect to n are zero:

$$\frac{\partial u}{\partial n} = \frac{\partial c}{\partial n} = \frac{\partial k}{\partial n} = \frac{\partial \varepsilon}{\partial n} = 0 \tag{17}$$

where n is the component of the normal vector on the water surface. The velocity component cross the water surface is zero and the pressure deviation is zero at the water surface. Thus the following boundary conditions are obtained,

$$\frac{\partial F}{\partial t} + u \frac{\partial F}{\partial x} - w = 0 \tag{18}$$

$$p' = 0 \tag{19}$$

where F expresses the form of the water surface. For the analysis of the density underflow, the set of the partial differential equations(1) to (6) with Eq.(7) will be solved using the boundary conditions (8) to (19) numerically. The equations are discretized by the SIMPLE method that Patankar [3] developed. This method is superior to the other method in the numerical stability. The calculation was carried out as follows. First, the values except for k and ε are assumed to be zero. The initial values of k and ε are set to be $k = 0.001 cm^2/s$ and $\varepsilon = 0.001 cm^2/s^3$, respectively. Then, the unsteady calculation are carried out. The steady solution is obtained after all variables are not changed with time.

Results of numerical solutions and discussions

In this section, the numerical solutions are compared with the experimental data obtained by Fukushima and Takashima [9] [10]. The experiment has been carried out by the measurement of the two-velocity component laser dopper anemometer. The distributions of velocity and salinity

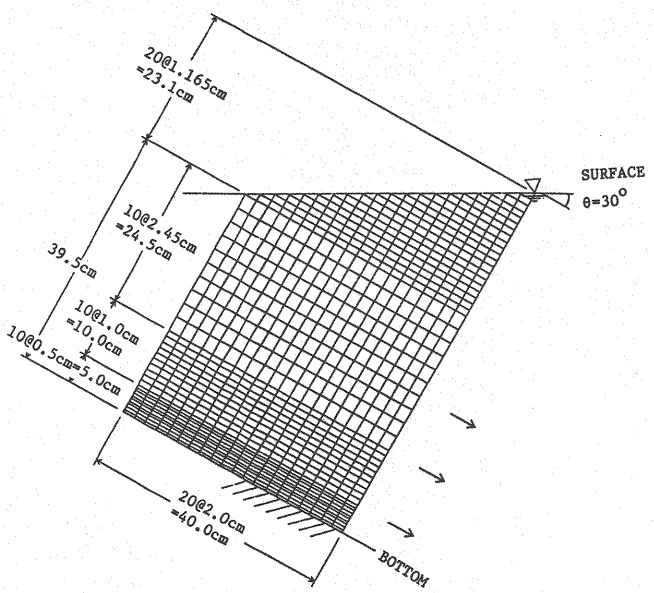

Fig. 2 Mesh arrangement.

concentration and the turbulent properties such as the kinetic energy of turbulence, the Reynolds stresses and the eddy viscosity are obtained by the experiment. The experimental apparatus is an acrylic water tank of 8.5 cm width, of 180 cm length and of 100 cm depth and the inclined solid plate of the 30° slope angle. The slot of 50 cm length and of 4 cm x 8.25 cm cross section is used. The tank is full of the fresh water and the saline water flows from the slot to form the inclined wall plume (or density underflow). The experimental conditions are the average velocity of 16.4 cm/s and the initial relative density difference of 0.0102. The Reynolds number is 6.7×10^3. The velocity is measured by the two-velocity component layser doppler anemometer. The water is sampled by the siphon and the salinity of sampled water is measured by the conductivity meter. The density is evaluated from the salinity concentration.

The calculational domain is taken by 40 cm in the x coordinate from the slot ($x = 0$ cm) and the bed to the water surface in the z direction (the maximum is $z = 62.6$ cm). The whole domein is divided into 20 nodes in the x-direction, and 50 nodes in the z-direction. Variable sizes of mesh are used in the calculation as shown in Fig. 2.

The velocity component of x-direction in the whole calculational domain is shown in Fig. 3. It is shown in the figure that the main body of flow is near the bed and the inverse flow resulting from the entrainment of the ambient water is simulated. The calculation of Fukushima and Takashima [9] [10] cannot explain this inverse flow, but the present analysis can as shown in Fig. 3. However, the reverse flow is weak so that we cannot compare the numerical solution with experimantal data.

Fig. 4 to Fig. 9 are comparison of the numerical solutions with the experimental data. Fig. 4 depicts the mean velocity distribution in the x- direction, Fig. 5 the distribution of the salinity concentration, Fig. 6 the distribution of the kinetic energy of turbulence, Fig. 7 the distribution of the Reynolds stresses, Fig. 8 the viscous dissipation rate of turbulence and Fig. 9 the distribution of eddy viscosity. In these figures, the solid lines indicate the numerical solution and the circles the experimental data. The numerical solution of velocity distribution explains well the experimental data as shown in Fig. 4. The numerical solution of the salinity concentration as shown in Fig. 5 is, however, smaller than the experimental data especially in the upper part. The reason of this is not clear. However, the assumption that the values of the parameter are the same as those of the non-stratified flow is doubtful. It is recommended that the optimum values of σ_t and $c_{3\varepsilon}$

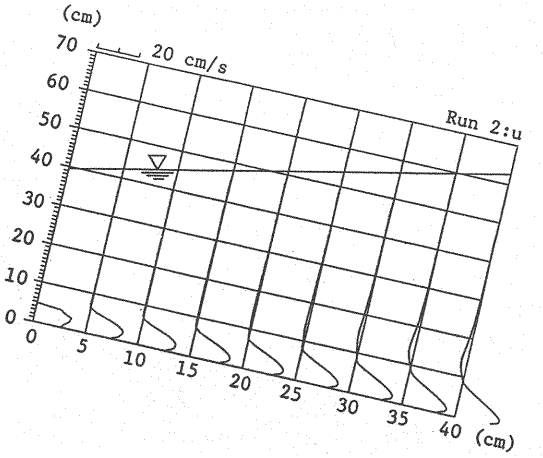

Fig. 3 The velocity component of the x direction in the whole domain.

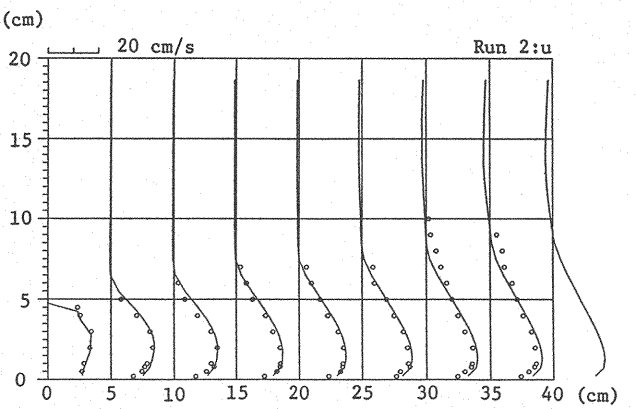

Fig. 4 Mean velocity distribution in the x direction. Circles indicate the experimental results. Solid line indicates the numerical calculation.

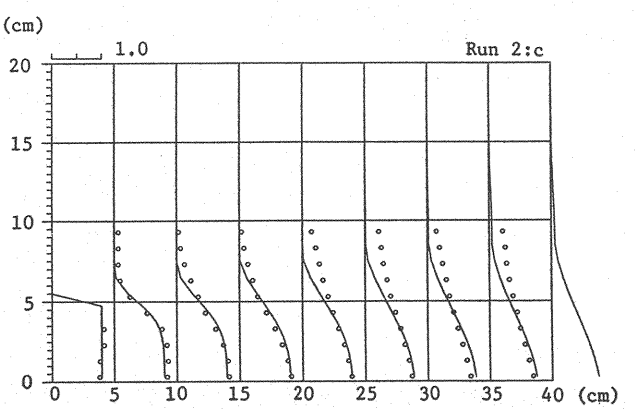

Fig. 5 Distribution of the salinity concentration. The symbols are the same as Fig. 4.

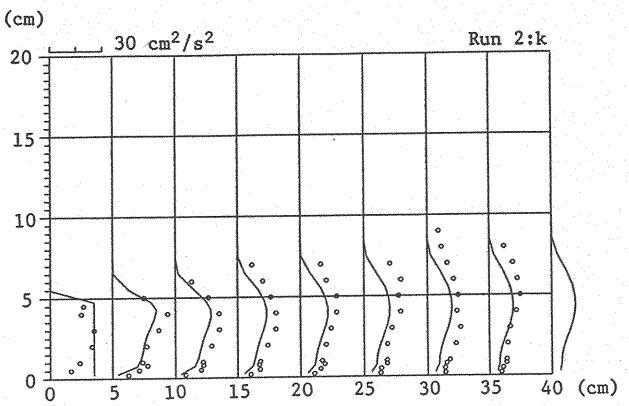

Fig. 6 Distribution of the kinetic energy of turbulence. The symbols are the same as Fig. 4.

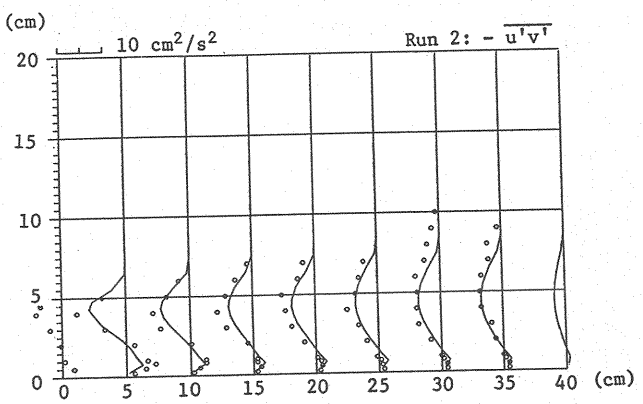

Fig. 7 Distribution of the Reynolds stress. The symbols are the same as Fig. 4.

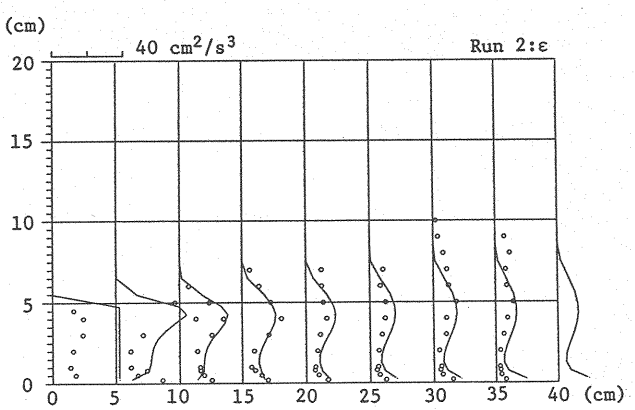

Fig. 8 Distribution of the viscous dissipation rate of turbulence. The symbols are the same as Fig. 4.

will be found by the numerical calcuation in which the values of parameters are changed. The concentration fluctuations were not measured in the experiment. Therefore, the correlation of velocity and concentration fluctuations cannot be compared.

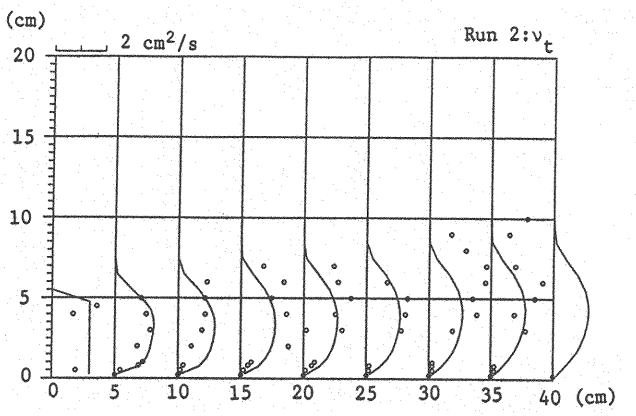

Fig. 9 Distribution of the eddy viscosity. The symbols are the same as Fig. 4.

Fig. 6 to Fig. 9 show distributions of turbulent properties. It should be taken into consideration that these experimental data are not accurate compared with the mean quantity. The eddy viscosity is calculated from the following relation:

$$\nu_t = -\overline{u'v'}/(\partial u/\partial z) \tag{20}$$

The Reynolds stresses and the gradient of the velocity is not accurate enough. The distribution of the kinetic energy of turbulence calculated are generally small compared with the experimental data as shown in Fig. 6. On the other hand, the numerical solution of the Reynolds stress agrees well with experimental data as shown in Fig. 7. This is the reason that agreement between the numerical solution and the experimental data of the mean velocity is fairly well. The distribution of viscous dissipation rate ε are compared with the experimental data as shown in Fig. 8. The experimental data are obtained from the -5/3 power law of the power spectrum of the velocity fluctuation. The upper part of the experimental data of the viscous dissipation rate is larger than the numerical solution. This tendency is the same as that of the concentration distribution. Therefore, the values of the parameters used in this calcuation are not appropriate, espetially the value of σ_t. The experimental data of the eddy viscosity as shown in Fig. 9 is considerably scatterd. This reason is mentioned before. It is difficult to discuss the applicability of the numerical solution of the eddy viscosity to the experimental data.

Conclusion

The calculation of the flow development region of density underflow is carried out using the $k-\varepsilon$ turbulence model. The numerical solution explains the main body of the underflow and the inverse flow resulting from the entrainment of the ambient water. The numerical solution also explains well turbulent properties such as the kinetic energy of turbulence, the Reynolds stresses the viscous dissipation rate of turbulence and the eddy viscosity. However, the accuracy of the turbulent properties in the experiment is still doubtful. More accurate experiment will be necessary to compare with the numerical solution.

This model will be developed to solve the motion of the head region of unsteady density underflow.

References

[1] Ellison, T.H. and J.S. Turner : Turbulent entrainment in stratified flows, Journal of Fluid Mechanics, Vol.6, pp.423-448, 1959.

[2] Tsubaki, T. and T. Komatsu : Flow properties of turbulent entrainment of stratified incline plume, Proceedings of Japanese Conference on Hydraulics, Vol.23, pp.415-422, 1979.

[3] Rodi, W. : Turbulence Model and Their Application in Hydraulics, State of Arts Paper, IAHR, 1980.

[4] Ljuboya, M. and W. Rodi : Prediction of horizontal and vertical turbulent buoyant wall jet, Trans. ASME, J. Heat Transfer, Vol.103, pp.343-349, 1981.

[5] Grella, J.J. and G.M. Faeth : Measurement in a two-dimensional thermal plume along a vertical adiabatic wall, Journal of Fluid Mechanics, Vol.71, part 4, pp.701-710, 1975.

[6] Sini, J.F. and I. Dekeyser : Numerical prediction of turbulent plane jets and forced plumes by use of $k-\varepsilon$ model of turbulence, International Journal of Heat Mass Transfer, Vol.30, No.9, pp.1787-1801, 1987.

[7] Murota, A., K. Nakatsuji and Y. Fujisaki : Calculation of vertical mixing in two-dimensional turbulent buoyant surface jet with turbulence model, Proceedings of Japan Society of Civil Engineers, Vol.411, No.II-12, pp.35-44, 1989.

[8] Fukushima, Y. : Analysis of inclined wall plume by turbulence model, Proceedings of Japan Society of Civil Engineers, Vol. 399, No. II-10, pp. 65-74, 1988.

[9] Fukushima,Y. and T. Takashima : Development region of wall buoyant jet, Technical Report of Nagaoka University of Technology, Vol. 11, pp. 45-52, 1989.

[10] Fukushima, Y. and T. Takashima : Analysis of development region of density underflow by turbulence model, Proceedings of Japanese Conference on Hydraulics, Vol. 33, pp.589-594, 1989.

[11] Fukushima, Y. and T. Takashima : Turbulent measurement of two-dimensional inclined wall plume, Proceedings of Japan Society of Civil Engineers, Vol. 411,No. II-12, pp. 259-262, 1989.

[12] Patankar, S.V. : Numerical Heat Transfer and Fluid Flow, Hemispere Publishing Co., 1980.

[13] Rajaratnam, N. : Turbulent Jets, Elsevior Scientific Publishing Co.,Amsterdam, 1976.

Appendix-Notation

The following symbols are used in this paper;

- A_s = numerical constant in the log-law;
- $c_{1\varepsilon}$ = coefficient in ε-equation (Eq.6);
- $c_{2\varepsilon}$ = coefficient in ε-equation (Eq.6);
- $c_{3\varepsilon}$ = coefficient in ε-equation (Eq.6);
- c_μ = coefficient in Eq.(7);
- D = molucular diffusivity;
- F = shape of water surface;
- g = gravity acceleration;
- h = depth of the flow;
- k = kinetic energy of turbulence;
- n = coordinate normal to the water surface;
- p' = pressure deviation from the hydrostatic pressure distribution;
- R = ratio of the salinity concentration to the relative density difference;
- u = velocity component in the x direction;
- u_* = shear velocity;

w = velocity component in the z direction;
x = coordinate in the main flow direction;
z = coordinate normal to the x direction;
z_o = height z near the bed;
ε = viscous dissipation rate of turbulence;
θ = slope angle of the channel;
κ = Kármán constant;
ν = kinematic viscosity;
ν_t = eddy viscosity;
ρ = density of the saline water;
ρ_o = density of the fresh water;
σ_t = turbulent Schmidt number for salinity;
σ_k = turbulent Schmidt number for kinetic energy of turbulence and
σ_ε = turbulent Schmidt number for viscous dissipation rate of turbulence.

(Received April 27, 1990; revised July 17, 1990)